Optimal and Modular Configuration of Wind Integrated Hybrid Power Plants for Off-Grid Systems

Lennart Petersen*†, Florin Iov*, German C. Tarnowski†, Carlos Carrejo†
*Department of Energy Technology, Aalborg University, Denmark.
†Vestas Wind Systems, Denmark
Email: lep@et.aau.dk, fi@et.aau.dk, getar@vestas.com, cecgo@vestas.com

***Abstract*—This paper focusses on the system configuration of off-grid hybrid power plants including wind power generation. First, a modular and scalable system topology is proposed. Secondly, an optimal sizing algorithm is developed in order to determine the installed capacities of wind turbines, PV system, battery energy storage system and generator sets. The novelty of this work lies in a robust sizing algorithm with respect to the required resolution of resource data in order to account for intra-hour power variations. Moreover, the involvement of the electrical infrastructure enables a precise estimation of power losses within the hybrid power plant as well as the consideration of both active and reactive power load demand for optimally sizing the plant components. The main outcome of this study is a methodology to determine feasible system configurations of modular and scalable wind integrated hybrid power plant solutions for off-grid applications.**

***Index Terms*—Hybrid power plant; wind power; solar photovoltaic; battery energy storage; generator set; optimal sizing; system configuration; techno-economic analysis.**

I. Introduction

In a global perspective particularly in emerging and frontier markets, a significant trend is to be expected towards distributed energy systems to ensure rural electrification. This means that the traditional power system structure (bulk generation → transmission → distribution → consumption) moves away towards a distributed cellular architecture, where a number of small-scale off-grid systems are collecting power from a number of distributed generation assets and providing power for local consumers. These off-grid systems can be preferred for instance due to geographic reasons in remote locations (islands, regions with low population density, secluded industrial sites) or for political, commercial or social reasons. The key advantage of off-grid systems is that power is produced closer to the consumption premises to prevent investments in the electricity transmission systems.

Traditionally, the power generation in off-grid systems has been based on fossil-fueled production systems (i.e. diesel generators) which need to account for logistics, storage and availability of fuels in remote areas. However, it is shown in many studies that the most cost effective approach for providing energy is to combine multiple distributed energy resources (DERs), e.g. wind turbines (WTGs), photovoltaic (PV) and battery energy storage systems (BESSs) [1], [2], [3], [4].

One of the most important aspects for so-called off-grid hybrid power plants (HPPs) is the configuration architecture. It determines the system topology and location, installed capacity and generic system management strategies according to the estimated power demand and the desired security of supply level [5]. The majority of research activities in this area have focussed on techno-economic analyses using state-of-the-art commercial software (e.g. HOMER Pro®) in order to determine the optimal sizing of an off-grid HPP, based on a given load demand profile on site with a specific system topology [3], [4]. None of the studies has focused on a modular and scalable approach for configuring a HPP with wind power and other DERs.

The state-of-the-art sizing method is to perform the techno-economic analysis by using hourly mean values of load demand and renewable resource data (wind speed and solar irradiation). It has not been investigated yet, how accurate a system configuration can be determined based on hourly mean values due to the potential necessity of operational reserve. This reserve is required due to the intra-hour power variations caused by wind speed fluctuations, varying load demand as well as cloud effects in the solar irradiation.

The majority of studies perform a pure energy analysis by representing active power generation vs. demand. Another important aspect is the supply of reactive power demand to the demand subsystem, which has an effect on the plant configuration according to the studies in [6] due to limited reactive power capacities of the individual DERs. This feature is not available in commercial software solutions, mostly due to the omission of the system electrical infrastructure.

The contribution of this paper is to address a methodology to determine feasible system configurations of modular and scalable wind integrated HPP solutions for off-grid applications. The novelty of this work lies in a robust sizing algorithm with respect to the required resolution of resource data in order to account for intra-hour power variations. Moreover, the involvement of the electrical infrastructure enables a precise estimation of power losses within the HPP as well as the consideration of both active and reactive power load demand for optimally sizing the HPP components.

This study will focus on off-grid HPPs including WTGs, PV, BESS and gensets. The size category relates to the most common user applications, i.e. residential and communities containing a mix of residential, commercial and small industrial consumers. In this context, the anticipated installed capacity of off-grid HPP, where production and consumption is in near proximity, is below 1 MW. However, another demanding user application for on-site off-grid HPPs is found in energy-intensive industry (e.g. pulp mill, cement kiln) or military bases [7]. Here the typical size of the required generation capacity is 5 - 100 MW, potentially up to 400 MW. Therefore, the aspect

of further upscaling to multi-MW level will be addressed in the end of this paper. In section II a modular and scalable system topology for the off-grid HPP is proposed. In section III the subsystem models of all HPP components are described, being used for developing an optimal sizing algorithm (section IV). Section V presents an assessment study with the aim of evaluating and improving the sizing algorithm in order to account for intra-hour power variations. In section VI the paper is concluded with some recommendations for the application and advancement of proposed methodology.

II. Modular and Scalable System Topology

In this section the study system is described, including system topology, the DERs as well as the different load types present in the HPP. Fig. 1 shows one HPP topology, which is entirely based on LV infrastructure.

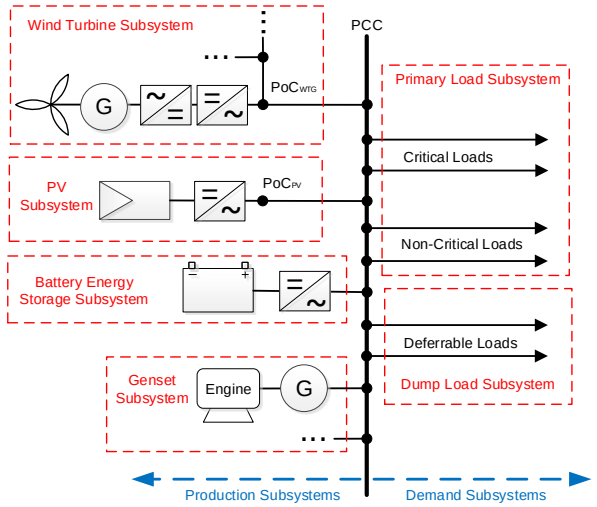

Figure 1. Generic single line diagram of a hybrid power plant topology, entirely based on LV infrastructure

A. Demand Subsystems

The main objective is the connection of end-customers to the supply connection point, i.e. the point of common coupling (PCC). The demand subsystems are indicated by numerous radial LV-feeders. Their characteristics are dependent on the actual community layout, the occurrence of feeder branching, the present consumers and electric parameters of cables and overhead lines. Critical (emergency) and non-critical (possibly sheddable) loads belong to the primary load subsystem as the aggregated electrical load that the system shall meet in order to avoid power shortage. Deferrable loads are assigned to the dump load subsystem, characterized by the excess electricity produced by the DERs in order to be used for deferrable consumption.

B. Production Subsystems

The connection of all DERs on the AC side provides the advantage that HPPs can be designed and expanded with standardized components on a flexible and modular basis [8]. Additionally, such HPP will be compliant with available regulatories for safety and protection [9]. In Fig. 1 the BESS and genset subsystem are directly interfaced with the PCC. The WTG and PV subsystem exhibit a separate point of connection (PoC), respectively. In most cases they need to be located further away from the community due to spacious constraints and natural resource requirements, i.e. wind conditions and exposure to solar irradiation. The interconnection with the PCC can be realized via overhead lines or cables (e.g. a few hundred meters up to several km). WTGs, PV arrays and batteries are grid interfaced via converters, such having the capability of delivering reactive power if required by the load. The prime movers of fuel based systems convert their energy usually via synchronous generators, which provide reactive power capability according to their power factor rating.

The system topology shown in Fig. 1 operates on one common voltage level. Thus the balance of plant has low CAPEX, as transformers can be avoided. However, due to the highly resistive characteristics of LV lines high OPEX is expected due to power losses. Moreover, the maximum distance between the PCC and the renewable energy sources (RES) is limited due to voltage drops across the lines. Fig. 2 illustrates this phenomenon, taking to account that the voltage drops should not exceed $\triangle V = 6\,\%$ [9]. As the characteristics depend highly on the selected line diameter (the higher the diameter, the smaller the resistance), the maximum distance depending on the actual power infeed from RES is shown for various commercially available line types. It can be remarked that larger line diameters enable more distant RES, however with the drawback of higher power losses (OPEX) and cable costs (CAPEX). If the WTG or PV subsystem's rated capacity was 70 kW, the maximum distance would be less than 250 meters with power losses of $S_{loss} = 1.53\,\%$, using a $25\,mm^2$-line. The distance can be increased towards 900 meters by choosing a $150\,mm^2$-line, however the corresponding line losses amount to $S_{loss} = 8.19\,\%$ which is unaccceptable. The aim of this study is to determine a HPP architecture that

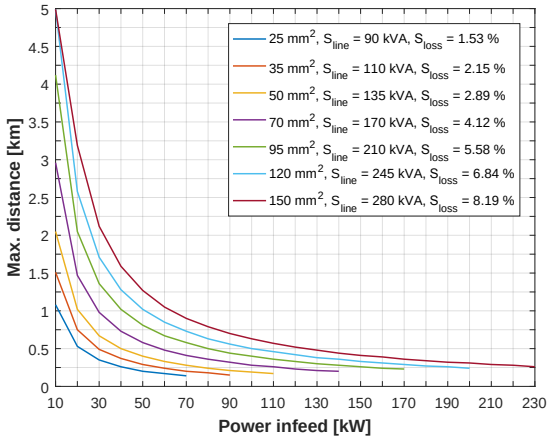

Figure 2. Maximum distance between RES and PCC according to various power infeeds and for different line diameters, accounting for a maximum voltage drop of $\triangle V = 6\,\%$

allows configuration of discrete DER modules and a certain

degree of scalability of the HPP by taking into account the expected demand growth over years. Hence, the most suitable system topology is presented in Fig. 3. A MV/LV substation transformer at the PCC acts as the grid connection interface of WTG and PV subsystem. The use of MV lines reduces the power losses and corresponding voltage drops. Moreover, a modular and redundant approach is realized by integrating step-up transformers on DER level. The choice of the MV level depends on the desired scalability of the HPP with regards to the installed RES capacity. Lower MV levels are preferred due to the involved cost of substation equipment (switchgear, transformers etc.). Fig. 4 shows the maximum possible distance

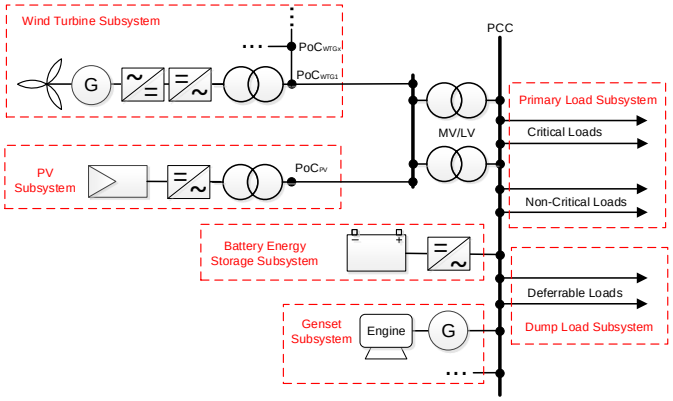

Figure 3. Generic single line diagram of the proposed hybrid power plant topology

(logarithmic scale) depending on the actual power infeed of the RES, for different common voltage levels. A maximum power infeed of 1000 kW is considered and takes into account that the double RES capacity may be required to supply the consumers of a rural community, where a peak power demand of more than 500 kW is not expected. The optimal voltage level depends on the expected RES power capacity and siting of WTG and PV subsystems. A 6.6 kV level will enable distances up to 4 km, even for high power infeed levels (900 kW). Additionally, it offers a flexible setup for the connection of gensets, as 6.6 kV is a common voltage level for diesel gensets rated above 800 kW [10].

Fig. 5 shows the expected power losses for such system topology. Depending on the power infeed from RES and the distance between RES and PCC, the power loss has a significant share of between 3 % and 6.5 %. Hence, it is to be expected that the power losses affect the energy analysis and need to be taken into account for the sizing algorithm to be developed.

III. Subsystem Models

This section describes the approach for modeling the individual system components. The focus is to capture the system dynamics which are relevant with respect to the operational scheduling with a maximum time resolution of 1 minute. First, the physical characteristics of the subsystems are described, whereupon the respective economic models are shortly summarized.

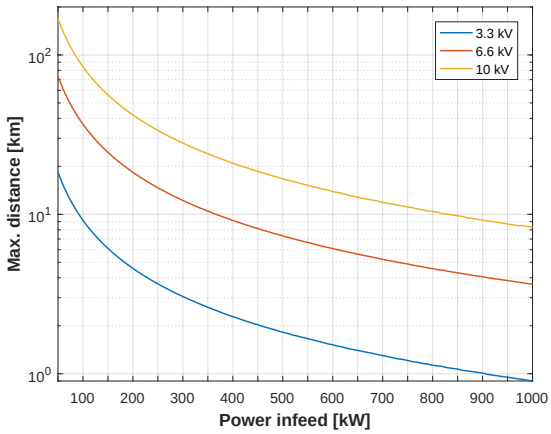

Figure 4. Maximum distance between RES and PCC according to various power infeeds for MV levels, accounting for a maximum voltage drop of $\triangle V = 6\,\%$

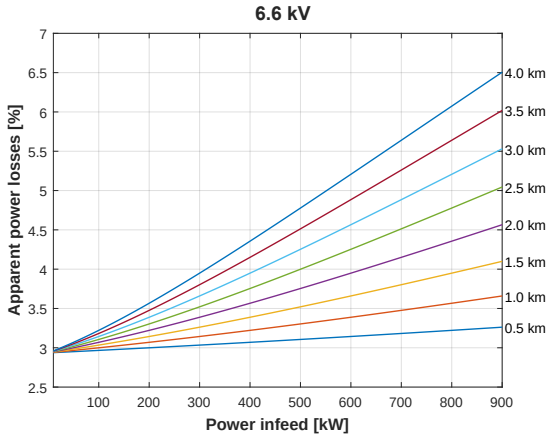

Figure 5. Apparent power losses according to various power infeeds and for different distances between RES and PCC

A. Physical Models

Fig. 6 presents a block diagram with the corresponding in- and outputs of all subsystem models.

In many areas, particularly in developing countries, very few information is available regarding the load demand of present electricity consumers. Hence, it is necessary to model the end-user's electric need in order to compute load demand profiles of the primary load subsystem. One method is proposed in [11], where end-consumers are grouped into different classes, which are defined by considering that consumers within the class show a similar demand behavior. Then, the present number n_{ij} of electrical appliances i within each user class j are described by means of power consumption P_{ij}, continuous functioning cycle d_{ij}, total functioning time h_{ij} and functioning windows ($h_{ij,start}$, $h_{ij,stop}$) during the day. In this way, the total required daily energy demand of each user class with specific number of users N_j and thereby the corresponding load profile for active power P_{PL} and reactive power Q_{PL} can be determined, taking into account the rated power factor $\cos\theta_{ij}$ of each electrical appliance.

The WTG's active power output P_{WTG} at its PoC is a function

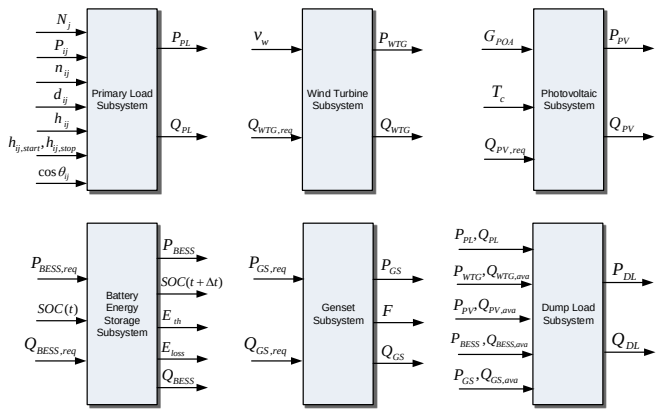

Figure 6. Block diagram of subsystem models

of wind speed v_w and is generally given by the turbine power curve. The PV's active power output P_{PV} at its PoC is mainly a function of the plane-of-array irradiance G_{POA} and the solar cell temperature T_c at the intended site. The power temperature coefficient model provides a comprehensive description of the characteristics and is given by Eq. 1

$$P_{PV} = \eta_{PV} \cdot \frac{G_{POA}}{G_{STC}} P_{PV,rat} \left[1 + \gamma \cdot (T_c - T_{STC})\right] \quad (1)$$

where η_{PV} is the power conversion efficiency, T_c the solar cell temperature, γ the temperature coefficient and G_{STC}, T_{STC} , $P_{PV,rat}$ the solar irradiance, the temperature and the rated peak power of the PV array under standard test conditions ($1000\,{}^{W}/_{m^2}$, $25\,C$).

The active power P_{BESS} of the BESS at its PoC depends mainly on the power request signal $P_{BESS,req}$, the BESS characteristics and the actual battery state $SOC(t)$. The characteristics of the BESS refer to the total storage capacity, the round-trip efficiency of the battery, the max. charging/discharging current of the battery as well as the total power rating and power losses of the converter system. In this study the maximum state-of-charge limit is assumed to be $SOC_{max} = 0.8\,\mathrm{pu}$, considering that the battery capacity degrades during the lifespan. The end-of-life criterium is commonly defined as, when the energy capacity has decreased by 20 %. The model output reveals the updated SOC at time $t + \Delta t$, the energy throughput E_{th} and the energy E_{loss} lost in the battery during the time period Δt. The reactive power outputs of WTG (Q_{WTG}), PV (Q_{PV}) or BESS subsystem (Q_{BESS}) depend on the requested signal ($Q_{WTG,req}$, $Q_{PV,req}$, $Q_{BESS,req}$) and the reactive power capability of the converter system. It is assumed that the system design of each converter interfaced DER (WTG, PV or BESS) shall account for minimum costs, i.e. overrating of components shall be avoided. In this way, the rated apparent power $S_{DER,rat}$ shall be equal to the rated power value of the DER, i.e. $P_{DER,rat}$. Then, the available reactive power of the DER $Q_{DER,ava}$ is depending on the actual power production as per Eq. 2.

$$Q_{DER,ava} = \sqrt{S_{DER,rat}^2 - P_{DER}^2} \quad (2)$$

This assumption may apply for kW-scale DERs. MW-scale DERs are generally designed to meet demanding grid code requirements and thereby have available increased converter ratings.

The genset active power output P_{GS} at its PoC is a function of the power request $P_{GS,req}$ subject to the minimum load ratio $f_{GS,min}$, which is the minimum allowable load on the generator during operation, expressed in per unit of its rated capacity $P_{GS,rat}$ (see Eq. 3). This constraint exists, since manufacturers recommend that their generators shall not run below certain load to avoid mechnical failures. A typical value is $f_{GS,min} = 0.3$.

$$P_{GS,min} = f_{GS,min} \cdot P_{GS,rat} \quad (3)$$

The fuel consumption F of the genset can be described by the linear fuel curve as per Eq. 4

$$F = F_0 \cdot P_{GS,rat} + F_1 \cdot P_{GS} \quad (4)$$

where F_0 is the generator fuel curve intercept coefficient in $\left[{}^{L}/_{h \cdot kW_{rated}}\right]$ and F_1 the generator fuel curve slope coefficient in $\left[{}^{L}/_{h \cdot kW_{output}}\right]$. Linear fuel curves are provided for many commercially available gensets [12]. However, in order to improve the accuracy of the genset fuel consumption, non-linear fuel curves are to be obtained. The reactive power output Q_{GS} of the genset is determined by the request signal $Q_{GS,req}$ and the generator capability curve. The reactive power capability is defined by the armature current limit, field current limit and end region heating limit of the generator [13].

The dump load is an equivalent of the excess power, when the generated power cannot be fully consumed by the primary load or stored in the BESS. One way is to curtail the RES during excess energy production, which requires from the WTGs and PV to be capable of regulating the power output (by blade pitching in case of WTGs). Another way is to use the energy to supply a deferrable load. The equivalent dump load active power profile P_{DL} and the remaining available reactive power Q_{DL} by all DERs is a result of the optimization algorithm described in the following section.

B. Economic Model

The economic model considers the capital, replacement, fuel, operation and maintanence costs as well as the salvage value of the subsystems. It requires knowledge about component costs and lifetimes as well as operational parameters (e.g. BESS energy throughput, genset fuel consumption). In this analysis, the discount factor is applied to calculate the present value of a cash flow that occurs in any year N of the project lifetime N_p. The discount factor f_d is calculated as per Eq. 5 and 6

$$f_d(N) = \frac{1}{(1 + r_1)^N} \quad (5)$$

$$r_1 = \frac{1 + r_2}{1 + r_3} - 1 \quad (6)$$

where N is the number of years and r_1, r_2 r_3 are the discount rate, interest rate and inflation rate, respectively. The total net present cost (NPC) of the HPP is determined by Eq. 7 as the

total of all subsystem costs, i.e. WTG, PV, BESS, genset as well as the substation and distribution lines.

$$C_{NPC,HPP} = C_{WTG} + C_{PV} + C_{BESS} + C_{BESS,con} + C_{GS} + C_{SS} + C_{LN} \quad (7)$$

The annualized cost $C_{ann,HPP}$ takes into account the capital recovery factor CRF, which is a ratio used to calculate the present value of an annuity (Eq. 8 and 9).

$$C_{ann,HPP} = CRF \cdot C_{NPC,HPP} \quad (8)$$

$$CRF = \frac{r_1 \cdot (1+r_1)^{N_p}}{(1+r_1)^{N_p} - 1} \quad (9)$$

The levelized cost of energy (LCOE) is calculated as the average cost per kWh of useful electrical energy produced by the system (Eq. 10)

$$LCOE = \frac{C_{ann,HPP}}{E_{PL,served}} = \frac{C_{ann,HPP}}{E_{PL} - E_{short}} \quad (10)$$

where E_{PL} and E_{short} are the total energy of primary load subsystem and the total energy shortage for one year, respectively.

IV. Optimal Sizing Algorithm

The developed optimization algorithm for sizing off-grid HPPs applies the subsystem and economic models described in previous sections. First, the optimization problem is formulated including decision variable, objective function and constraints. Subsequently, the individual simulation steps are explained.

A. Problem Formulation

The decision variables of the optimization algorithm refer to the ratings of the individual components, i.e. rated power $P_{WTG,rat}$ of the WTG subsystem, rated power $P_{PV,rat}$ of the PV subsystem, rated energy capacity $E_{BESS,rat}$ of the BESS subsystem, rated power $P_{BESS-con,rat}$ of the BESS converter, number of gensets n_{GS} , rated power $P_{GSx,rat}$ of the n-th genset and the substation transformer rating $S_{TR,rat}$. The decision variable vector is presented in Eq. 11.

$$\mathbf{X} = \begin{bmatrix} P_{WTG,rat} & P_{PV,rat} & E_{BESS,rat} & \\ P_{BESS-con,rat} & n_{GS} & P_{GSx,rat} & S_{TR,rat} \end{bmatrix} \quad (11)$$

The optimization problem is formulated such as to minimize $LCOE$, subject to the constraints of Eq. 12 - 13.

$$LPSP \leq LPSP_{max} \quad (12)$$

$$\mathbf{X} \in \chi \quad (13)$$

where χ is the feasibility region of the decision variables and the LPSP is the probability of insufficient power supply for the present load demand and is expressed by the sum of time when the HPP is not able to supply the load demand vs. the total observed time (e.g one year) as per Eq. 14

$$LPSP = \frac{\sum_{t=1}^{T} \{\Delta t_f \; for \; (P_S(t) < P_{PL}(t)) \; or \; (Q_S(t) < Q_{PL}(t))\}}{T} \quad (14)$$

where T, Δt_f, $P_S(t)$, $Q_S(t)$, $P_{PL}(t)$ and $Q_{PL}(t)$ are the total observed time period (one year), the time period of power failure, the supplied active and reactive power as well as the active and reactive power demand of the primary load subsystem, respectively.

B. Simulation Steps

The algorithm for determining the optimal sizes of the DERs within the HPP follows an enumeration-based single-objective optimization approach. The corresponding flowchart is shown in Fig. 7 and comprises three major stages, i.e. initialization, simulation and post-processing. The general algorithm sequence for the simulation and post-processing stage is based on the work in [6]. However, in this study an additional focus is laid on the initialization stage to limit the search space for accelerated computational performance. Moreover, the detailed algorithms for two operational strategies are developed and applicable for the wind integrated HPP being in scope of this study.

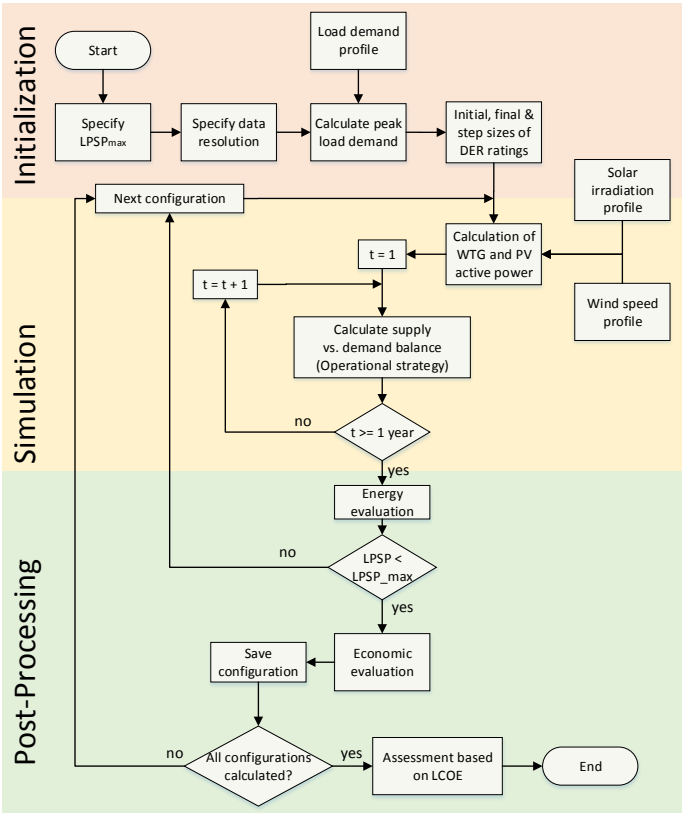

Figure 7. Flowchart of optimal sizing algorithm

B.1 System Initialization

The objective of the system initialization process is to define the search space of the decision variables. Here, the aim is to limit the search space to the minimum required in order to reduce the computational time of the algorithm. In this way, the following steps impose additional constraints to the optimization problem.

The system initialization begins with specifying the permitted loss of power supply probability $LPSP_{max}$ as well as the data resolution of the simulation. The state-of-the-art approach is to use hourly mean values. However, if more granular data of the wind and solar resource as well as the load demand are available, the time intervals can be reduced down to 1 minute. In the next step, the initial value, final value and step sizes of the decision variables are specified. The maximum size of WTG subsystem $P_{WTGs,rat,max}$ and PV subsystem $P_{PV,rat,max}$ are determined according to the required annual energy consumption. It is expected that the total required energy produced by WTG or PV subsystem, respectively, will not exceed the total energy consumption, so that Eq. 15 and 16 are applied

$$P_{WTGs,rat,max} = \left\lceil \frac{E_{PL}}{E_{WTG,1kW} \cdot P_{WTG,rat}} \right\rceil \cdot P_{WTG,rat} \tag{15}$$

$$P_{PV,rat,max} = \left\lceil \frac{E_{PL}}{E_{PV,1kW}} \right\rceil \tag{16}$$

where $E_{WTG,1kW}$ and $E_{PV,1kW}$ is the total energy produced by 1 kW WTG and PV subsystem, respectively, measured in ${}^{kWh}/_{kW}$. The final numbers are rounded up towards integer numbers of feasible ratings. Then, the number x of discrete variables within the search space ($\left[0 : \frac{P_{WTGs,rat,max}}{x-1} : P_{WTGs,rat,max}\right]$ and $\left[0 : \frac{P_{PV,rat,max}}{x-1} : P_{PV,rat,max}\right]$) is selected according the desired granularity. Note, that there is a trade-off between accuracy and computational time. The aggregated rating of both substation transformers is selected according to the installed RES capacity as per Eq. 17. In this way, system redundancy and future expansion of the RES subsystem is ensured.

$$S_{TR,rat} = 2 \cdot (P_{WTG,rat} + P_{PV,rat}) \tag{17}$$

The step size $E_{BESS,rat,step}$ of the BESS capacity rating is selected in order to supply the average load consumption for 1 hour, as per Eq. 18.

$$E_{BESS,rat,step} = \left\lceil \frac{E_{PL}}{8760} \right\rceil \tag{18}$$

The search interval with number x of discrete variables within the search space is determined as $[0 : E_{BESS,rat,step} : (x-1) \cdot E_{BESS,rat,step}]$. During the assessment studies it is observed that the maximum required BESS capacity does not exceed 8 hours of the average load consumption ($x = 9$).

As the cost of power electronics has become relatively low, the BESS converter rating is selected to supply the peak load demand in time periods with low wind speed and solar irradiation and to avoid the start-up of genset units (see Eq. 19).

$$P_{BESS-con,rat} = \lceil P_{PL,peak} \rceil \tag{19}$$

With regard to sizing the genset subsystem, it is anticipated that various feasible setups need to be investigated, as there is a trade-off between OPEX, redundancy and fuel costs depending on number of gensets in the HPP. Concerning the level of required maintenance, one genset is favorable compared to numerous gensets. However, the redundancy increases with the number of available gensets. The fuel expenses depend on the minimum load ratio and the fuel efficiency curve of the respective genset. One important advantage of having numerous gensets running in parallel is expandability on a modular basis in case of load demand growth during the project lifetime.

The individual ratings of the gensets respect the commercially available products. In the range between 10 - 100 kW products are available with an interval size of 10 kW, while for systems larger than 100 kW the possible increment is 50 kW. Following scenarios are considered to ensure 100 % power supply availability for time periods with very low renewable generation and low SOC of the BESS:

- *One genset to cover the peak load demand.*
- *Two gensets with equal ratings to cover the peak load demand.*
- *Three gensets with equal ratings to cover the peak load demand.*

B.2 System Simulation and Post-Processing

The simulation begins by obtaining the annual active power profiles of WTG and PV subsystem respectively by using the models described in section III. Subsequently, the balance of demand vs. supply is calculated during each time step of a whole year by using one of the operational strategies described in the following subsection. The post-processing of a certain system configuration contains the calculation of the key parameters such as $LPSP$. If the permitted value for $LPSP_{max}$ is violated, the corresponding system configuration is discarded and the simulation is repeated with updated decision variables of the DERs. The economic evaluation is accomplished by using the economic models described in previous section. Finally, the decision variables of all system configurations are assessed based on the resulting LCOE of the HPP.

B.3 Operational Strategy - Load Following

The operational strategy is a set of rules used to schedule the operation of the BESS and, if present, gensets whenever there is insuficient power from RES to supply the primary load demand. The most common operational strategies are the *Load Following (LF)* strategy and the *Cycle Charging (CC)* strategy [12]. By applying the *LF* strategy, whenever a genset operates, it produces only sufficient power to meet the primary load demand. Under the *CC* strategy, whenever a genset is required to operate to supply the primary load, it operates at rated output power. The *LF* strategy tends to be optimal in systems with a lot of renewable power, when the renewable power output sometimes exceeds the load [12]. In contrast, the *CC* strategy tends to be optimal in systems with little or no renewable power, which does not apply for the HPPs investigated in this study. The aim of this study is to extend the state-of-the-art strategies in order to represent both active and reactive power flow within the HPP. Hence, the models of the operational strategies are formulated with the aim of maintaining for each time step the balance of active and reactive power. Whenever

these equations cannot be solved due to insufficient active or reactive power by the DERs, an event of power shortage occurs. The DERs are utilized to meet the primary load demand in the following sequence of priority: 1. PV and WTG subsystem, 2. BESS subsystem, 3. Genset subsystem (if present). It is chosen to prioritize the RES subsystems for supplying the reactive power demand, since the BESS and genset subsystem shall have enough Q availability to compensate the short-term power fluctuations.

Fig. 8 shows the algorithmic flowchart of the *LF* strategy. First, the reactive power outputs of WTG and PV subsystem are determined. $Q_{PV}(t)$ and $Q_{WTG}(t)$ are calculated according to the required load demand $Q_{PL}(t)$ and the available reactive power $Q_{PV,ava}(t)$ and $Q_{WTG,ava}(t)$. Then the effective active power $P_{RES,PCC}(t)$ and reactive power $Q_{RES,PCC}(t)$ at the LV side of the substation (the PCC) are obtained according to Eq. 20 - 24. The total power generation $S_{RES}(t)$ at the sending end of the distribution subsystem amounts to:

$$\begin{aligned} S_{RES}(t) &= P_{RES}(t) + jQ_{RES}(t) = P_{WTG}(t) \\ &\quad + P_{PV}(t) + j\left(Q_{WTG}(t) + Q_{PV}(t)\right) \end{aligned} \tag{20}$$

Then the voltage $V_{RES}(t)$ at the sending end is calculated as per Eq. 21 [14].

$$\begin{aligned} V_{RES}(t) &= V_{PCC} + \frac{R_{DS}P_{RES}(t) + X_{DS}Q_{RES}(t)}{V_{RES}(t)} \\ &\quad + j\frac{X_{DS}P_{RES}(t) - R_{DS}Q_{RES}(t)}{V_{RES}(t)} \end{aligned} \tag{21}$$

where R_{DS} and X_{DS} are the resistance and reactance of distribution lines and substation transformers. As the PCC voltage is assumed to be regulated to $V_{PCC} = 1\,\mathrm{pu}$, the sending end voltage is obtained by Eq. 22.

$$\begin{aligned} V_{RES}(t) &= \frac{V_{PCC}}{2} + \sqrt{\frac{V_{PCC}}{4} + R_{DS}P_{RES}(t)} \\ &\quad \overline{+X_{DS}Q_{RES}(t) + j\left(X_{DS}P_{RES}(t) - R_{DS}Q_{RES}(t)\right)} \end{aligned} \tag{22}$$

The current flowing through the distribution subsystem amounts to:

$$I_{DS} = \frac{S^*_{RES}(t)}{V^*_{RES}(t)} \tag{23}$$

Finally, the effective power at PCC is obtained by Eq. 24.

$$\begin{aligned} S_{RES,PCC}(t) &= P_{RES,PCC}(t) + jQ_{RES,PCC}(t) \\ &= V_{PCC} \cdot I^*_{DS} \end{aligned} \tag{24}$$

When there is a surplus of power generation from RES ($P_{PL}(t) < P_{RES,PCC}(t)$), it is used to charge the BESS. The charging capability of the BESS depends on its SOC, charging rate and converter rating, resulting into a maximum charging power $P_{BESS,max,ch}$. When surplus power cannot be fully stored, then the remaining power is supplied to the dump load.

When there is a power deficit ($P_{PL}(t) > P_{RES,PCC}(t)$), the BESS is discharged up to its maximum discharging power $P_{BESS,max,dch}$. If the BESS cannot deliver sufficient power, an event of power shortage occurs, unless gensets are present in the HPP. In this case ($n_{GS} > 0$), the genset goes into operation and supplies the remaining primary load demand. Due to the load ratio constraint of an operating genset, the delivered power may exceed the deficit power $P_{def}(t)$. Thus, the remaining power by the genset is used to charge the BESS.

If the power of BESS and primary genset are not sufficient to meet the load demand, an event of power shortage occurs, unless several gensets is available ($n_{GS} > 1$). Any further genset follows the same logic as the primary genset, i.e. its operational state is determined in order to follow the primary load demand.

When the reactive power demand cannot be fulfilled by RES, the BESS available reactive power is utilized to supply the deficit $Q_{def}(t)$. An event of reactive power shortage occurs, if the BESS rating is reached, unless gensets are present in the HPP. In this case, the reactive power capability of the genset is utilized. Only, if the reactive power deficit cannot be compensated, an event of reactive power shortage occurs, unless a furtherd genset is available to contribute with additional reactive power.

C. Algorithm Validation

The purpose of this section is to present representative simulation results in order to validate the performance of the sizing algorithm. The proposed algorithm in this study is validated against the simulation platform HOMER Pro®. An exemplary load demand profile including residential, commercial (e.g. enterprises, mobile charging stators, kiosks, school, pharmacy) and small industrial consumers (e.g. grain mills, repair shops) is applied and renewable resource data from a site in Kenya/Africa with high wind conditions are used in this study. Some assumptions are made due to the design limitations in HOMER Pro®. E.g. it is not possible to include the electrical infrastructure of the distribution subsystem (i.e. substation transformers and distribution lines), as the design specification is limited to the DER components. Hence, the distance between RES subsystems and PCC is neglected during the simulations and the costs of any substation and lines are not taken into consideration. Moreover, it is not possible to account for reactive power load demand. Hence, the simulations are limited to an energy analysis based on the balance of active power supply and demand.

The results of the first four computed system configurations are compared by means of Fig. 9. It is noteworthy that both proposed algorithm and HOMER Pro® obtain the same configurations, however in different sequence with respect to the lowest LCOE. Fig. 9 shows that the computed values for LCOE are comparable with small errors below 1 %, which is within an acceptable range. The measured computational time of proposed algorithm is around 7 minutes on average, which is acceptable. Hence, the chosen enumeration based approach for solving the optimization problem is satisfactory and more complex evolutionary algorithms are not required.

V. Assessment Study

In this section, the impact of the resolution of resource data on the ability of the configured HPP to supply the load demand is assessed by evaluating the LPSP criterion. The base case is to use hourly mean data ($\triangle t = 1\,\mathrm{h}$). Higher resolution data

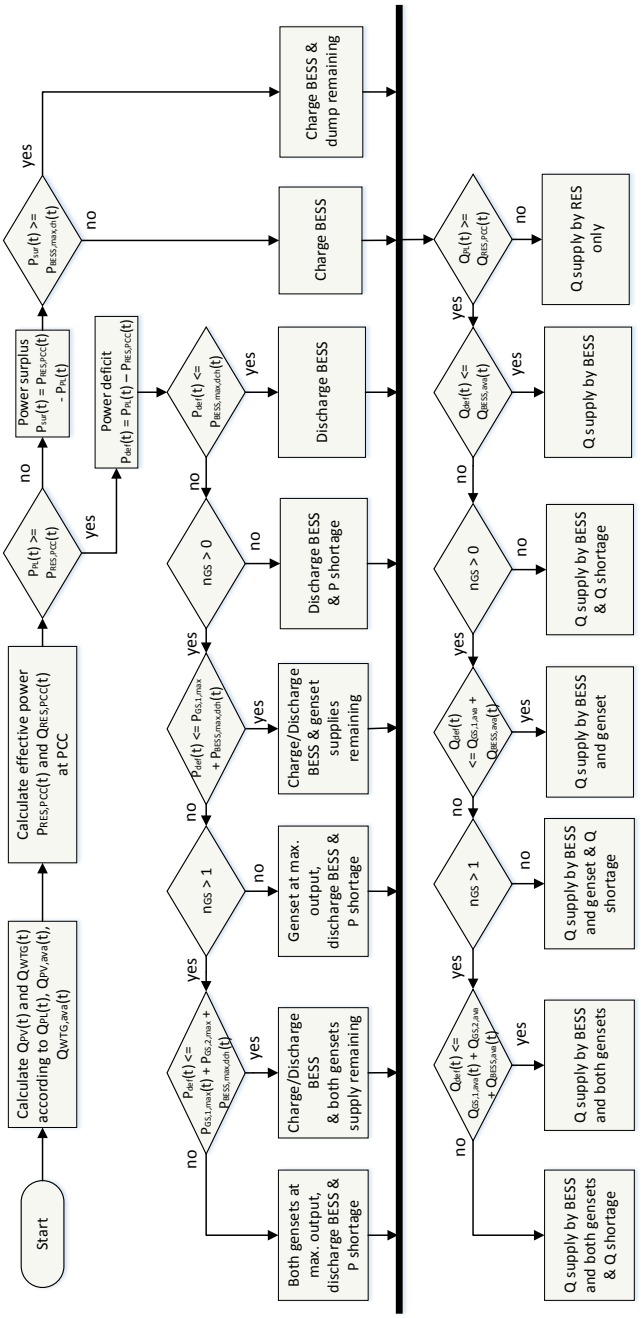

Figure 8. Flowchart of *Load Following* strategy

sets are available and used during the simulation in order to account for intra-hour power variations:

- $\triangle t = 10\,\mathrm{min}$
- $\triangle t = 5\,\mathrm{min}$
- $\triangle t = 1\,\mathrm{min}$

A. Simulation Results for Base Case

The computed system configuration involving 60 kW WTG subsystem, 80 kW PV, 160 kWh/90 kW BESS and 3 x 30 kW gensets is the cost optimal solution with an LCOE of $0.1902\,{}^{\$}/_{kWh}$, simulated with hourly mean values. In this study case, the electrical infrastructure of the HPP is taken into

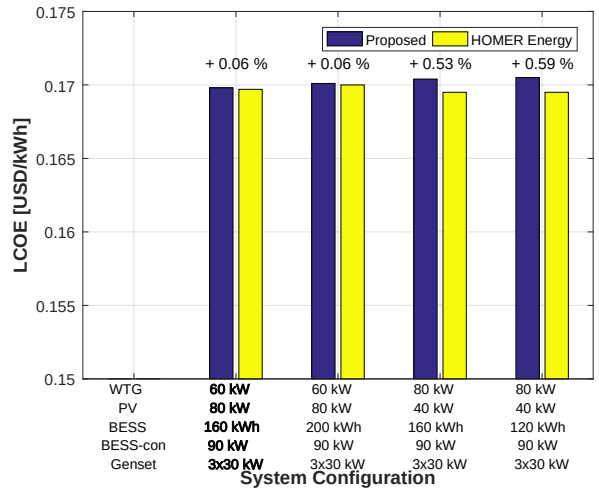

Figure 9. Result comparison for the computed system configurations

account, assuming a distance of 1 km between RES subsystems and PCC. Subsequently, this particular HPP is evaluated for higher time resolutions, however with unaltered production profile of the genset subsystem. Here, the assumption is that unit commitment and economic power dispatch of diesel generators in smaller time intervals than 1 hour may not be desired in practice due to wear and tear during start ups / shut downs and constantly changing operating points.

The results for the obtained LPSP during the simulations are summarized in Tab. I, where $LPSP > 0$ indicates events of power shortage. It can be remarked that events of power

Table I
SIMULATION RESULTS FOR BASE CASE AND TUNED CASE

Time resolution Δt	1 h	10 min	5 min	1 min
LPSP [%] for Base Case	0.00	2.20	1.96	1.33
LPSP [%] for Tuned Case	0.00	0.00	0.00	0.00

shortage occur for higher time resolutions, which is related to the intra-hour power fluctuations as demonstrated in Fig. 10. Here, relavant time domain profiles are shown for an exemplary hour of the year with present power shortage. At this operating point for $\triangle t = 1\,\mathrm{h}$, the SOC of the BESS is nearly at its minimum level of $SOC_{min} = 0.2$. For higher time resolutions the SOC approaches the 1 h mean value at the time of 15.45 h. The WTG and PV production in the next few minutes is highly volatile and predominantly deceeding the hourly average value. Hence, the load demand cannot be fulfilled (power shortage), as the energy capacity of the BESS is drained and the genset will only go into operation at the next full hour (16.00 h).

B. Algorithm Tuning

In order to avoid these power shortage events, sufficient operational power reserve is required. The approach is to provide reserve power by the BESS, as it is the most flexible DER unit in the system due to constant operation and the capability to quickly balance out mismatches between power supply and demand $\Delta P(t) = P_S(t) - P_{PL}(t)$. Presently, the operating

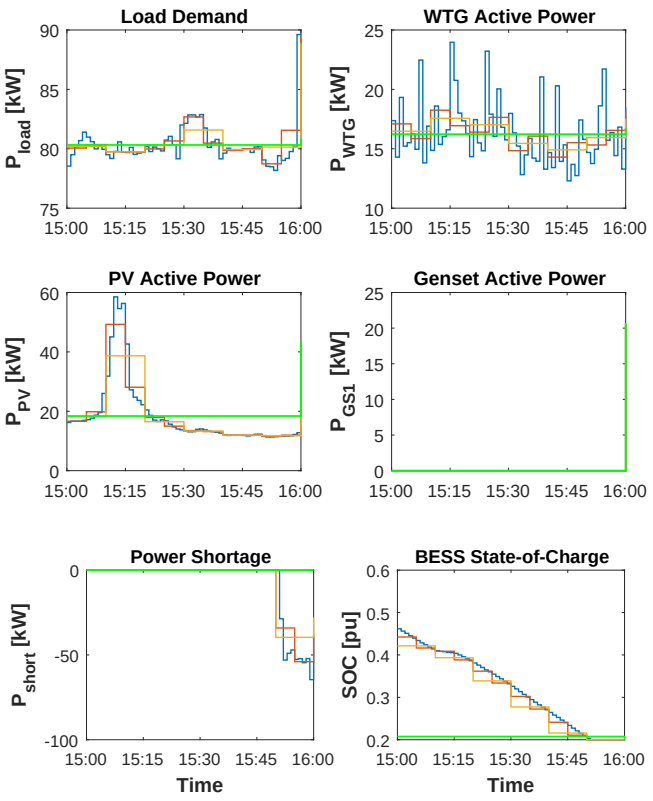

Figure 10. Base Case: P_{PL}, P_{WTG}, P_{PV}, P_{GS1}, P_{short}, SOC, for various time resolutions (green = 1 h, yellow = 10 min, red = 5 min, blue = 1 min)

interval for the BESS is defined between $0.2 < SOC < 0.8$. On the one hand, reducing the maximum limit SOC_{max} can account for positive $\Delta P(t)$. This, however will reduce the long-term charging capability being required for storing excess power production of RES throughout the day. A more economical way of dealing with short-term overproduction is RES curtailment. On the other hand, increasing the minimum limit SOC_{min} can ensure sufficient power supply during negative $\Delta P(t)$. The required operational reserve is determined based on statistical analysis carried out in the following sequence:

- Calculate the vectors for remaining power to be supplied after delivering WTG and PV power as per Eq. 25, for $\triangle t = 1\,\mathrm{h}$ and $\triangle t = 1\,\mathrm{min}$.

$$\mathbf{P_{rem,\Delta t}} = \mathbf{P_{PL,\Delta t}} - \mathbf{P_{WTG,\Delta t}} - \mathbf{P_{PV,\Delta t}} \qquad (25)$$

- Determine the vector for positive power mismatch as per Eq. 26.

$$\mathbf{dP} = \mathbf{P_{rem,1\,min}} - \mathbf{P_{rem,1\,h}} \;\; \{dP > 0\} \qquad (26)$$

- Calculate the power reserve $dP_{99\,\%}$, required for 1 hour time interval in 99 % of the cases, based on the empirical cumulative distribution expressed by Eq. 27 and shown in Fig. 11.

$$F(dP_{99\,\%}) = 0.99 \qquad (27)$$

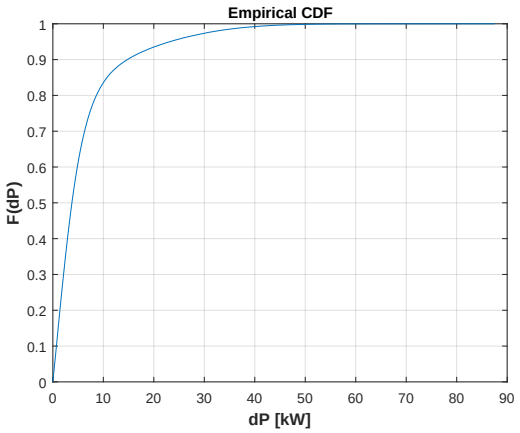

Figure 11. Empirical Cumulative Distribution for vector $\mathbf{dP}$

- Determine the updated minimum SOC limit as per Eq. 28.

$$SOC_{min,1\,h} = 0.2 + \frac{dP_{99\,\%} \cdot 1\,h}{E_{BESS,rat}} \qquad (28)$$

C. Simulation Results for Tuned Case

The hourly based simulation for the computed system configuration is repeated by using the updated SOC limit $SOC_{min,1\,h} = 0.44$. Compared to the untuned case, the unit commitment and power dispatch profile of the genset subsystem is altered due to the reduced available capacity of the BESS. This leads to an increased LCOE of $0.2020\,\$/kWh$ (+ 6 %). Subsequently, the system configuration is evaluated for higher time resolutions, however with default SOC limit of $SOC_{min} = 0.2$. Fig. 12 depicts the results for the time domain profiles of the same operating point as shown in Fig. 10. In this case, the genset is already in operation at time 15.00 h, as the updated SOC limit has been deceeded. Hence, the BESS is able to balance the intra-hour power variations, since sufficient energy capacity is available before reaching the absolute minimum SOC. No power shortage events are observed during the simulations as stated in Tab. I. Hence, the developed tuning process for the algorithm is valid in order for the configured HPP to supply the load demand in every minute of the year.

VI. Summary and Recommendations

The paper has presented a methodology to determine feasible system configurations of modular and scalable wind integrated HPP solutions for off-grid applications. In the first step, the composition of various components and the electrical infrastructure is defined to enable modularity and scalability of the HPP. The described balance of plant allows an installed RES capacity of up to 900 kW, being sited with a maximum distance of 4 km towards the PCC of the HPP. Upscaling towards multi-MW scale HPPs requires an enhanced voltage level for the MV lines between RES subsystem and PCC to account for power losses and the permitted voltage drops.

Subsequently, the assumptions for modelling the different components of the HPP are exposed. The loads, WTG, PV,

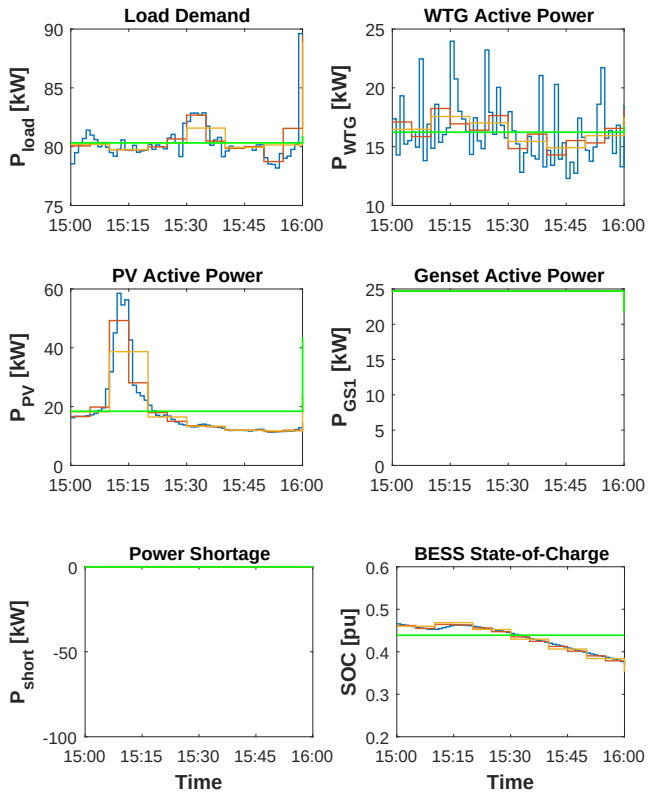

Figure 12. Tuned Case: P_{PL}, P_{WTG}, P_{PV}, P_{GS1}, P_{short}, SOC, for various time resolutions (green = 1 h, yellow = 10 min, red = 5 min, blue = 1 min)

BESS and genset subsystem are modelled from a technical and economical perspective according to the purpose of this study. The physical models have low bandwidth to simply represent active and reactive power flow on minute scale.

Finally, the developed optimization algorithm for sizing the HPP is explained in detail. The enumeration-based single-objective approach is divided in three stages, i.e. initialization, simulation and post-processing, being described by means of a flow diagram. One key development is obtained by intelligent definition of the search space during the system initialization in order to reduce the computational time of the simulation. The simulation itself considers supply of both active and reactive power demand as well as the power losses within the HPP.

The assessment study shows that it is necessary to provide certain amount of operational reserve to account for the intra-hourly power fluctuations due to changes in wind speed, solar irradiation and load demand. A methodology based on statistical data analysis is proposed for the BESS to provide power reserve by specifying an enhanced value for the minimum SOC. Future advancements of the proposed configuration algorithm shall be approached to account for very short-term dynamics on subsecond scale which are relevant for voltage and frequency stability within the HPP. Additional active and reactive power reserve may be required by the DERs in order to balance out voltage and frequency variations. This in turn can have an impact on the component sizing. In this study, the considerations concerning operational scheduling are based on the assumption that all resources are known by means of deterministic profiles. However, in practice the available renewable power generation as well as load consumption needs to be predicted in order to optimally dispatch BESS and gensets.

Upscaling towards multi-MW scale does not necessarily have an impact on the sizing algorithm. As diesel generators for off-grid systems can be up to 10 MW [7], it allows upscaling towards a maximum generation capacity of 30 MW without necessary advancements of the operational strategies. However, a high number of units is required for large-scale projects with 50+ up to hundreds of MW installed capacity. In this case, the genset subsystem will impose challenges due to the complexity of parallel genset operation. Here, the operational strategies need to account for more complex algorithms to ensure cost optimized load sharing between multiple gensets. Additionally, in the presence of large fixed speed motor loads, special attention needs to be paid to the active and reactive power rating of the DERs in order to cope with high inrush currents during start up and the increased reactive power demand of highly inductive loads.

Acknowledgment

This work was carried out as part of the PhD project “Proof-of-Concept on Next Generation Hybrid Power Plant Control”. The authors acknowledge Innovation Fund Denmark for financial support through the Industrial PhD funding scheme.

References

[1] Rajesh Kumar, R. A. Gupta, and Ajay Kumar Bansal. Economic analysis and power management of a stand-alone wind/photovoltaic hybrid energy system using biogeography based optimization algorithm. *Swarm and Evolutionary Computation*, 8:33–43, 2013.

[2] A. Maitra, L. Rogers, and R. Handa. Program on Technology Innovation: Microgrid Implementations: Literature Review. Technical report, Electric Power Research Institute, 2016.

[3] Omar Hafez and Kankar Bhattacharya. Optimal planning and design of a renewable energy based supply system for microgrids. *Renewable Energy*, 45:7–15, sep 2012.

[4] Emilio Ghiani, Claudia Vertuccio, and Fabrizio Pilo. Optimal sizing of multi-generation set for off-grid rural electrification. In *IEEE Power and Energy Society General Meeting*, volume 2016-Novem, pages 1–5. IEEE, jul 2016.

[5] Hengwei Lin, Chengxi Liu, Josep M Guerrero, Juan C Vasquez, and Tomislav Dragicevic. Modular Power Architectures for Microgrid Clusters. In *International Conference on Green Energy (ICGE)*, 2014.

[6] Faruk A Bhuiyan. *Optimal Sizing and Power Management Strategies of Islanded Microgrids for Remote Electrification Systems*. PhD thesis, University of Western Ontario, Canada, 2014.

[7] Ruud Kempener, Olivier Lavagne, Deger Saygin, Jeffrey Skeer, Salvatore Vinci, and Dolf Gielen. Off-Grid Renewable Energy Systems: Status and Methodological Issues. Technical report, 2015.

[8] SMA. *Solar Stand-Alone Power and Backup Power Supply*. Juwi Solar GmbH, 2009.

[9] IEC 62257. Recommendations for renewable energy and hybrid systems for rural electrification - Part 9-2: Integrated systems - Microgrids. Technical report, 2016.

[10] Mitsubishi. Power Generation generator sets - 400 kVA to 15 MW. Technical report, 2013.

[11] Stefano Mandelli, Claudio Brivio, Emanuela Colombo, and Marco Merlo. Effect of load profile uncertainty on the optimum sizing of off-grid PV systems for rural electrification. *Sustainable Energy Technologies and Assessments*, 18:34–47, dec 2016.

[12] HOMER Pro Version 3.7 User Manual. Technical report, HOMER Energy, Boulder, USA, 2016.

[13] University of Wisconsin. Estimating Generator Capability Curves. Technical report, 2015.

[14] A Keyhani and M Marwali. *Smart Power Grids*. 2011.